Detecting apoptosis *in vivo* and *ex vivo* using spectroscopic OCT and dynamic light scattering

Golnaz Farhat[a,b], Anoja Giles[b], Adrian Mariampillai[c], Victor X. D. Yang[b,c], Gregory J. Czarnota[a,b,d,e] and Michael C. Kolios[f]

[a]Medical Biophysics, Univ. of Toronto, Canada;
[b]Imaging Research, Sunnybrook Health Sciences Centre, Toronto, Canada;
[c]Electrical & Computer Engineering, Ryerson University, Toronto, Canada;
[d]Radiation Oncology, Sunnybrook Health Sciences Centre, Toronto, Canada;
[e]Radiation Oncology, Univ. of Toronto, Toronto, Canada
[f]Physics, Ryerson University, Toronto, Canada;

ABSTRACT

We present an *in vivo* implementation of a multi-parametric technique for detecting apoptosis using optical coherence tomography in a mouse tumor model. Solid tumors were grown from acute myeloid leukemia cells in the hind leg of SCID mice and treated with a single dose of cisplatin and dexamethasone to induce apoptosis. Both spectral features and speckle decorrelation times indicated good consistency between control mice and reasonable agreement with *in vitro* measurements. The integrated backscatter increased significantly in tumors responding to treatment while the spectral slope and decorrelation time did not show significant changes. This study demonstrates the feasibility of using spectroscopic OCT and dynamic light scattering for treatment monitoring *in vivo*.

Keywords: cell death, apoptosis, optical coherence tomography, spectroscopic, dynamic light scattering, speckle decorrelation, acute myeloid leukemia, treatment monitoring, *in vivo*.

1. INTRODUCTION

Apoptosis is a form of cell death often observed in tumor tissues as a result of cancer treatment such as chemotherapy or radiation therapy. It is characterized by a series of predictable and dynamic morphological changes within the cell, which occur as early as 24 to 48 hours after the start of treatment. Detection of apoptosis in treated tissues could permit treatment monitoring, identifying patients who are not showing an early response to treatment and providing the option of treatment modification at an early stage in the therapeutic process. Since it has been shown that early response can be a reliable indication of overall response[1,2], apoptosis detection may play an important role in improving treatment outcomes in cancer patients.

Light scattering methods have frequently been used to study subcellular structure[3,4]. These methods are sensitive to variations in cell morphology because the imaging wavelengths are on a similar scale to subcellular structures. Interferometric techniques including low coherence interferometry, digital holography and optical coherence tomography (OCT), have successfully been used to study cell morpholog[5], variations in intracellular motion[6] and cell death[7].

During apoptosis the cell undergoes a reduction in volume, condensation of the nucleus, nuclear and mitochondrial fragmentation and, finally, fragmentation of the cell itself into apoptotic bodies. Such variations in cell morphology modify the optical properties of tissue because of changes in the size, shape and distribution of subcellular structures. We have shown that significant differences in signal intensity and spectral properties can be measured[8] in cell samples undergoing apoptosis. Moreover, because this morphological transformation is a dynamic process occurring during a specific time window, we have demonstrated that variations in the OCT speckle intensity can be measured as a function of time[9].

Biomedical Applications of Light Scattering VIII, edited by Adam Wax, Vadim Backman, Proc. of SPIE Vol. 8952, 89520K · © 2014 SPIE
CCC code: 1605-7422/14/$18 · doi: 10.1117/12.2040075

In the current study we present an *in vivo* implementation of a multi-paramatric OCT technique for detecting apoptosis. Through the extension of a previously developed *in vitro* cell death model into an *in vivo* mouse tumor model we demonstrate the feasibility of using our method for *in vivo* detection of apoptosis.

2. METHODS

2.1 Cell culture and tumor model

The AML cells used in this study (AML-5, Ontario Cancer Institute, Toronto, Canada) were started from frozen stock samples and grown at 37^{o} C in suspension flasks containing 150 mL of α-minimal essential medium supplemented with 1% streptomycin and 5% fetal bovine serum. For all *in vitro* measurements, tightly packed cell samples were prepared using a method previously described[10].

The *in vivo* cell death model consisted of AML tumors grown in the hind leg of SCID mice. Each tumor was grown from 2 x 10^6 cells in 100 μl of phosphate buffered saline (PBS). This cell suspension was injected subcutaneously into the right hind leg of each of 18 mice (CB-17 SCID, Charles River, Canada). Tumors measuring approximately 5 mm in diameter developed over 17 days. Each mouse was randomly designated to one of three groups: control, 48 hours post-treatment and 72 hours post-treatment. The mice in the latter two groups were treated with dexamethasone (32 mg/65 kg) and cisplatin (150 mg/m^2), administered slowly and consecutively via a tail vein catheter. Saline was administered subcutaneously immediately following the chemotherapeutic agents. Prior to imaging, the skin overlying the tumor was removed to permit direct imaging access to the tumor tissue. The mice in the control group were imaged on day 1 (the day treatment was administered), while the treated mice were imaged at 48 hours or 72 hours post treatment. Immediately after imaging, the mice were sacrificed and tumors excised for the acquisition of an additional set of *ex vivo* data. All procedures, including surgeries, chemotherapy and imaging were conducted under ketamine (150 mg/kg) and xylazine (10 mg/kg) aneasthesia, administered subcutaneously and with institutional approval at Sunnybrook Health Sciences Centre (Toronto, Canada).

2.2 Data acquisition and analysis

All data were acquired in the form of 14-bit OCT interference fringe signals using a custom made swept-source OCT system similar to one described previously [11]. The system used in this study is based on a 36-facet polygon filter (Lincoln Laser Corp., Phoenix, AZ) and operates at a central wavelength of 1310 nm with in-air axial and lateral resolutions of 7.5 μm and 13.7 μm, respectively.

Two-dimensional (2D) data sets containing 128 axial scans (covering a transverse distance of 1 mm) were collected from each tumor in 10 planes spaced in such a way as to cover the entire tumor volume. Every effort was made to ensure that the tissue surface was located at the same distance with respect to the focal plane to maintain consistency between measurements. From each data set, a region of interest (ROI) starting at 50 μm beneath the tumor surface and measuring 250 μm axially by 780 μm laterally was selected. The lateral dimension was chosen to give approximately 100 a-lines per 2D image, while the axial dimension coincides with the depth of focus of the system. Spectroscopic OCT parameters, including the integrated backscatter (IB) and the spectral slope (SS) were calculated by summing the area underneath, and the slope of, the normalized backscatter spectrum, respectively. Details of this calculation have been described previously[8].

A second set of data was collected for the dynamic light scattering measurements. A series of two-dimensional frames containing 32 axial scans were recorded covering a transverse distance of 400 μm at a frame rate of 111 Hz. The field of view and number of a-scans, in this case, were minimized in order to maximize the frame rate. A ROI measuring 400 μm laterally by 50 μm axially (starting at 50 μm beneath the tumor surface) was selected. The decorrelation time (DT) at each image pixel within this ROI was obtained by calculating the autocorrelation of the signal intensity as a function of time and extracting the line width at 1/e of the maximum autocorrelation value. The details of this calculation have been described previously[9].

All of the above data acquisitions and calculations were repeated for each animal after the tumor was excised post-sacrifice. Therefore, for each tumor, measurements were made *in vivo* and *ex vivo*. Additionally, the same measurements were acquired from three untreated (control) AML cell samples for comparison.

2.3 Histological validation

Immediately after imaging tumors were fixed in 10% buffered formalin for 48 hours. Subsequently, the tissue was processed for haematoxylin and eosin (H&E) staining. Microscopy was carried out using a Leica DC 200 digital imaging system (Leica Microsystems GmbH, Germany).

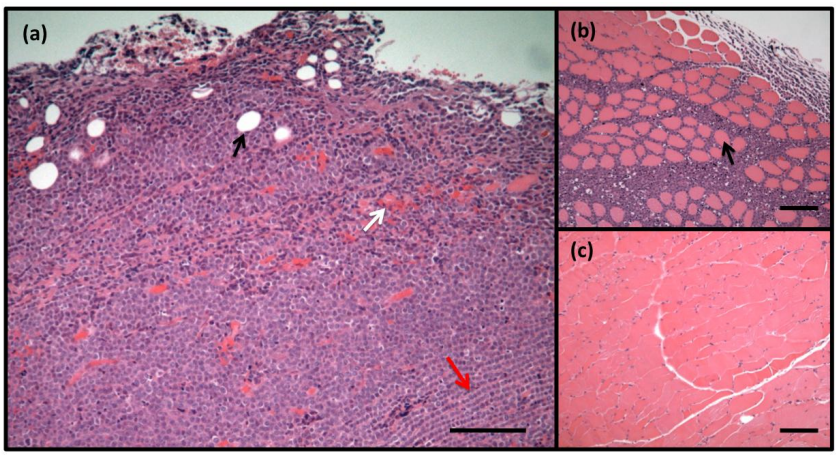

Figure 1. Variations in tumor structure. (a) Section of AML tumor stained with H&E revealing a heterogeneous microstructure. Arrows indicate the presence of vacuoles (black), blood vessels (white) and areas of cells organized in rows (red). (b) Section of tumor in which AML cells have invaded muscle tissue (muscle tissue indicated by black arrow). (c) Section of tissue in which no tumor growth is present, only muscle tissue is visible. Scale bars indicate 100 μm.

3. RESULTS AND DISCUSSION

3.1 Variations in tumor microstructure and treatment response

Digital images acquired from H&E stained tumor sections revealed a large variation in tumor microstructure both within a given tumor and between animals. Examples are highlighted in Figure 1(a) where the presence of vacuoles and variations in vasculature and cell organization are evident. We also observed cases in which the tumor cells had infiltrated neighboring muscle tissue (figure 2(b)) or where the tumor failed to develop completely (figure 2(c)). While heterogeneous tumor structure is a realistic expectation in a clinical setting, we wanted to maintain consistency between animals. Therefore, the extreme cases where no tumor developed or where muscle tissue was infiltrated (a total of 5 animals – 1 from the control group, 2 from the 48 hour treatment group and 2 from the 72 hour treatment group) were eliminated from the study.

3.2 Controls

We compared OCT parameters (IB, SS and DT) acquired from untreated AML tumors to those from control AML cell samples to determined whether our *in vivo* results would be consistent with *in vitro* measurements from the same cell line. The spectroscopic parameters (IB and SS) were calculated from both *in vivo* and *ex vivo* data and are plotted in Figure 2 (a) and (b). *In vivo* dynamic light scattering measurements were complicated due to respiratory motion. Despite stabilizing the hind leg of the mouse using surgical tape, in the majority of animals, possibly due to the administration of generalized anesthetic, the respiratory motion was very strong. For this reason, only the *ex vivo* data has been included in the analysis of the decorrelation data (Fig 2 (c)). We have previously used a window chamber model for in vivo DT measurements[12]. The window chamber is less prone to motion artefacts as it is more easily isolated and stabilized since the tumor is physically contained within the window. The motivation behind using the hind leg tumor model in this study is to allow for future multi-modality imaging using ultrasound, which requires a larger tumor volume.

The spectroscopic parameters show good consistency between animals as well as between *in vivo* and *ex vivo* measurements for each animal. This indicates that despite variations in tumor microstructure and the presence of blood flow we can obtain consistent results using these parameters. Furthermore, reasonable agreement is observed between *in vivo / ex vivo* results and those obtained *in vitro*. This may suggest that AML cells, even in the presence of blood cells, blood vessels and other tissue components, are responsible for the bulk of the OCT signal in these tumors. Further experimental investigation is needed to confirm this finding.

The DT parameter varies slightly between animals and is overall lower in the *ex vivo* tumor measurements compared to the *in vitro* cell samples. This discrepancy is not surprising as the presence of blood (even *ex vivo*) introduces an additional source of scatterer motion, causing a faster speckle decorrelation, and thus a shorter DT. Intracellular motion is largely dependent on cell metabolism and available growth factors. These conditions can be very different in a tumor versus a highly controlled *in vitro* environment. This can also explain the better consistency between the *in vitro* controls vs the *ex vivo* controls for this parameter, as the former were derived from a highly controlled environment while the latter were derived from a highly heterogenous and variable tumor environment.

Despite slight discrepancies observed with the DT measurement, the overall consistency of the control measurements of IB, SS and DT *in vivo,* and the agreement observed between parameter values acquired from *in vivo*, *ex vivo* and *in vitro* samples indicate the feasibility of using this technique for *in vivo* measurements.

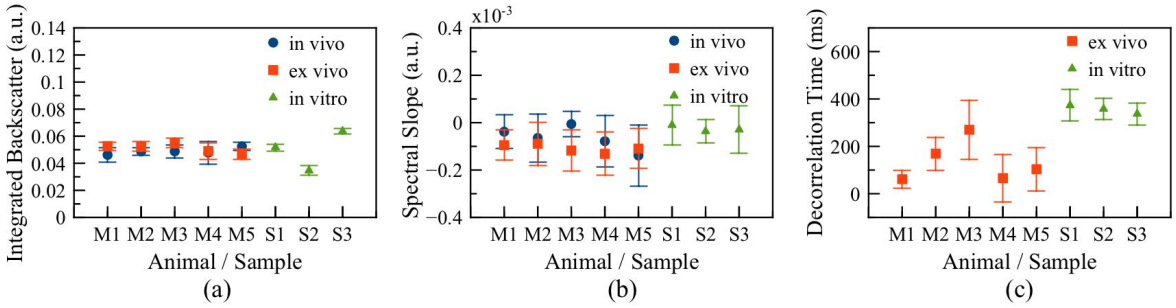

Figure 2. Comparing untreated animals to control cell samples. Integrated backscatter (a), spectral slope (b) and decorrelation time (c) results for 5 untreated mice (M1 through M5) and 3 control cell samples (S1 through S3). The IB and SS values are plotted for both *in vivo* and *ex vivo* measurements. The *in vivo* measurements for DT are not included.

3.3 Detecting apoptosis

Based on a qualitative assessment of the histological data, the treatment response in this study was neither consistent across all animals, nor as strong as the response we previously observed *in vitro*[8]. To the best of our knowledge, this is the first time this tumor model has been used in combination with a cisplatin/dexamethasone treatment. It is not a conventional tumor model as AML cells rarely form solid tumors, however it provided an opportunity to implement an *in vivo* model that could be directly compared to previous detailed *in vitro* studies. Due to the variability in the treatment response and in order to analyze the parameter results calculated from the treated tumors, we studied the H&E slides from each tumor and classified each animal as either a "responder" or a "non-responder". As indicated in Figure 3, "responders" were identified as tumors in which a significant number of cells displayed the characteristic morphological features of apoptosis such as nuclear condensation and fragmentation. This resulted in a total of 3 animals being classified as responders and 5 as non-responders.

The resulting parameter averages per group are plotted in Figure 4. The IB is significantly higher in the responder group when compared to the control and non-responder groups (0.068 ± 0.016, 0.049 ± 0.006 and 0.045 ± 0.008, respectively). The SS increased slightly for the responder group, however, this difference is not statistically significant. Finally, the DT does not indicate any significant difference between groups. These results suggest that the IB parameter is the most robust and can detect apoptosis *in vivo* (and *ex vivo*) in this tumor apoptosis model. The SS and DT, despite showing significant differences between treated and untreated cell samples in previous *in vitro* studies[8,9], do not clearly differentiate between tumors responding or not responding to treatment. One possible explanation for this may be the weak and variable treatment response.

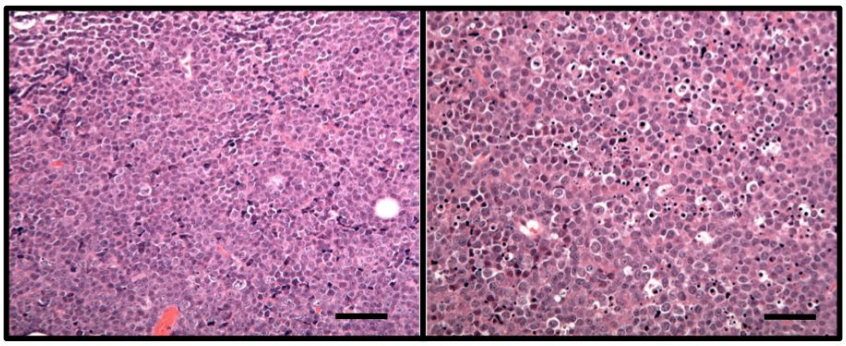

Figure 3. Representative H&E stained sections from AML tumors treated with cisplatin and dexamethasone. Tumors were classified as non-responders in the absence of apoptotic features (left) or responders if apoptotic hallmarks such as nuclear condensation and fragmentation were observed (right). Scale bars indicate 50 μm.

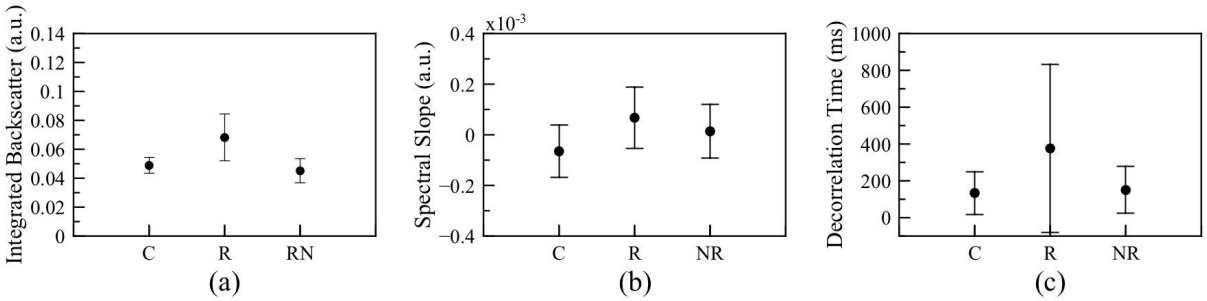

Figure 4. Integrated backscatter (a), spectral slope (b) and decorrelation time (c) for control (C), responders (R) and non-responders (NR). The parameters were calculated from *in vivo* data for IB and SS and from *ex vivo* data for DT.

4. CONCLUSIONS

In summary, we have presented an *in vivo* implementation of a previously developed multi-parametric technique to detect apoptosis using OCT. The comparison of control measurements acquired from AML tumors and AML cell samples indicated good consistency between tumors both *in vivo* and *ex vivo*, as well as reasonable agreement with *in vitro* cell samples. Of the three OCT parameters (IB, SS and DT) the IB was the most robust and increased significantly in tumors that responded to the cisplatin-dexamethasone treatment, while the SS and DT did not change significantly. This is the first time, to our knowledge, that OCT has been used to detect apoptosis in a hind-leg mouse tumor model. Despite limitations of the model such as large tumor microstructure variability and weak treatment response, this study has demonstrated the feasibility of using spectroscopic OCT and dynamic light scattering for *in vivo* treatment monitoring. Future work involves improving the treatment response through modification of the treatment model to further study the ability of SS and DT to detect apoptosis.

5. ACKNOWLEDGMENTS

The authors would like to acknowledge Dr. Ahmed El Kaffas, Christina Kim, Priscilla Lai and Dr. Azza Al-Mahrouki for their technical support. This research was made possible by funding from NSERC and the Canada Research Chairs Program awarded to Dr. Michael Kolios as well as the Cancer Care Ontario Research Chair awarded to Dr. Gregory Czarnota. Funding to purchase the equipment was provided by the Canada Foundation for Innovation, the Ontario Ministry of Research and Innovation, and Ryerson University.

6. REFERENCES

[1] Esteva, F., and Hortobagyi, G., "Can early response assessment guide neoadjuvant chemotherapy in early-stage breast cancer?," Journal of the National Cancer Institute 100(8), 521 (2008).

[2] Pantaleo, M., Nannini, M., Maleddu, A., Fanti, S., Ambrosini, V., Nanni, C., Boschi, S., and Biasco, G., "Conventional and novel PET tracers for imaging in oncology in the era of molecular therapy," Cancer treatment reviews 34(2), 103–121 (2008).

[3] Chalut, K.J., Ostrander, J.H., Giacomelli, M.G., and Wax, A., "Light Scattering Measurements of Subcellular Structure Provide Noninvasive Early Detection of Chemotherapy-Induced Apoptosis," Cancer Research 69(3), 1199–1204 (2009).

[4] Mourant, J., Canpolat, M., Brocker, C., Esponda-Ramos, O., Johnson, T., Matanock, A., Stetter, K., and Freyer, J., "Light scattering from cells: the contribution of the nucleus and the effects of proliferative status," Journal of Biomedical Optics 5, 131 (2000).

[5] Graf, R., and Wax, A., "Nuclear morphology measurements using Fourier domain low coherence interferometry," Optics Express 13(12), 4693–4698 (2005).

[6] Jeong, K., Turek, J., and Nolte, D., "Speckle fluctuation spectroscopy of intracellular motion in living tissue using coherence-domain digital holography," Journal of Biomedical Optics 15, 030514 (2010).

[7] Meer, F.J., Faber, D.J., Aalders, M.C.G., Poot, A.A., Vermes, I., and Leeuwen, T.G., "Apoptosis- and necrosis-induced changes in light attenuation measured by optical coherence tomography," Lasers in Medical Science 25(2), 259–267 (2010).

[8] Farhat, G., Yang, V.X., Kolios, M.C., and Czarnota, G.J., "Cell death monitoring using quantitative optical coherence tomography methods"790713–790713–9 (2011).

[9] Farhat, G., Mariampillai, A., Yang, V.X.D., Czarnota, G.J., and Kolios, M.C., "Detecting apoptosis using dynamic light scattering with optical coherence tomography," Journal of Biomedical Optics 16(7), 070505 (2011).

[10] Farhat, G., Czarnota, G., and Kolios, M., "Detecting cell death with optical coherence tomography and envelope statistics (Journal Paper)," Journal of Biomedical … 16, 026017 (2011).

[11] Leung, M.K., Mariampillai, A., Standish, B.A., Lee, K.K., Munce, N.R., Vitkin, I.A., and Yang, V.X., "High-power wavelength-swept laser in Littman telescope-less polygon filter and dual-amplifier configuration for multichannel optical coherence tomography," Optics Letters 34(18), 2814–2816 (2009).

[12] Farhat, G., Mariampillai, A., Lee, K.K., Yang, V.X., Czarnota, G.J., and Kolios, M.C., "Measuring intracellular motion using dynamic light scattering with optical coherence tomography in a mouse tumor model"823002–823002–7 (2012).